

# Superconductivity versus quadrupole density wave in $\text{CeRh}_2\text{As}_2$

K. Semeniuk,<sup>1,\*</sup> D. Hafner,<sup>1</sup> P. Khanenko,<sup>1</sup> T. Lühmann,<sup>1</sup> J. Banda,<sup>1</sup> J. F. Landaeta,<sup>1</sup> C. Geibel,<sup>1</sup> S. Khim,<sup>1</sup> E. Hassinger,<sup>2,†</sup> and M. Brando<sup>1,‡</sup>

<sup>1</sup>Max Planck Institute for Chemical Physics of Solids, 01187 Dresden, Germany

<sup>2</sup>Technical University Dresden, Institute for Solid State and Materials Physics, 01062 Dresden, Germany

(Dated: February 3, 2023)

$\text{CeRh}_2\text{As}_2$  has recently been reported to host a unique quadrupole-density-wave (QDW) state at temperatures below  $T_0 \approx 0.4\text{ K}$  and a multi-phase heavy-fermion superconductivity with  $T_c = 0.26\text{ K}$ . The two superconducting (SC) phases, SC1 and SC2, observed for a magnetic field  $H$  parallel to the  $c$  axis of the tetragonal unit cell, have been interpreted as even- and odd-parity SC states, separated by a first order phase boundary at  $\mu_0 H^* = 4\text{ T}$ . Such parity switching is possible due to a strong Rashba spin-orbit coupling at the Ce sites located in locally non-centrosymmetric environments of the globally centrosymmetric lattice. Existing reports suggest a possibility of the QDW transition line joining the SC1-SC2 phase boundary at a multicritical point and propose an alternative interpretation of the transition at  $H^*$ : It separates a mixed SC+QDW (SC1) and a pure SC (SC2) states. Here, we present a detailed study of higher quality single crystals of  $\text{CeRh}_2\text{As}_2$ , showing much sharper signatures of the phase transitions at  $T_c = 0.31\text{ K}$  and  $T_0 = 0.48\text{ K}$ . We refine the  $T$ - $H$  phase diagram of  $\text{CeRh}_2\text{As}_2$  and demonstrate that  $T_0(H)$  and  $T_c(H)$  lines meet at  $\mu_0 H \approx 6\text{ T}$ , well above  $H^*$ , implying no influence of the QDW on the SC phase switching. We do not detect the QDW transition within the SC2 state. A basic analysis with the Ginzburg-Landau theory suggests that we have a weak competing interaction between the two order parameters.

$\text{CeRh}_2\text{As}_2$  is a newly discovered heavy-fermion superconductor with remarkable properties. It hosts a peculiar non-magnetic ordered state below the temperature of  $T_0 \approx 0.4\text{ K}$ , proposed to be a unique case of a quadrupole-density-wave (QDW) instability [1], contrasting all known multipolar orders observed in Ce-based systems, which are typically of local origin [2, 3]. More interestingly,  $\text{CeRh}_2\text{As}_2$  shows a multi-phase heavy-fermion superconductivity at an even lower temperature of  $T_c = 0.26\text{ K}$  [4]. Such a phenomenon is also exceptionally rare: Apart from  $\text{UPt}_3$  [5–7] and  $\text{UTe}_2$  [8–11], virtually all other unconventional superconductors host only one superconducting (SC) state. Above  $T_c$ , the compound shows a non-Fermi-liquid temperature dependence of specific heat,  $C/T \propto T^{-0.6}$ , and electrical resistivity,  $\rho(T) \propto \sqrt{T}$ , suggesting a proximity to a quantum critical point of unknown nature [4] or a presence of two-channel Kondo physics [12]. On top of this, recent nuclear quadrupolar resonance experiments have detected broadening of the As lines below  $T_N < T_c$ , but only at one of the two As sites, pointing to a presence of internal fields, likely due to an antiferromagnetic (AFM) order within the SC phase [13].

$\text{CeRh}_2\text{As}_2$  shows a single SC phase when magnetic field is applied along the basal plane of the tetragonal crystalline structure, but two SC phases, SC1 and SC2, for a field  $H$  parallel to the  $c$  axis (the relevant field direction for the rest of this paper). These phases are separated by a first order transition line at  $\mu_0 H^* = 4\text{ T}$ , as shown

in Fig. 1. The anisotropic field response of the superconductivity, as well as the presence of two SC phases in  $\text{CeRh}_2\text{As}_2$  can be explained by a model which takes into account a strong Rashba spin-orbit coupling due to locally non-centrosymmetric environments of the Ce sites and a quasi-two-dimensional character of the Fermi sur-

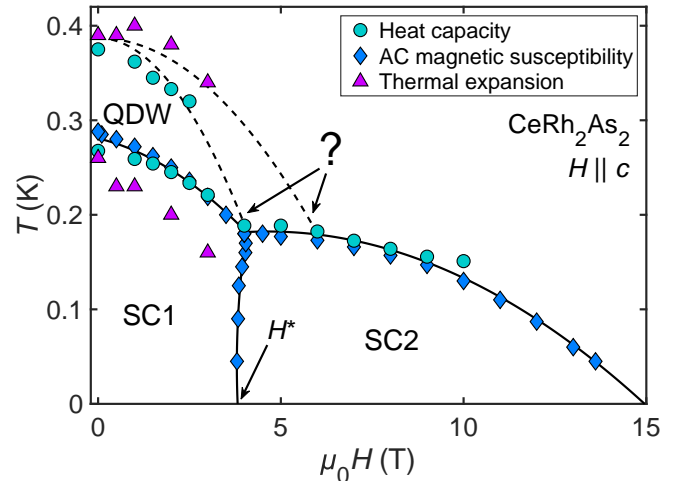


FIG. 1: Temperature -  $c$ -axis magnetic field ( $T$ - $H$ ) phase diagram of  $\text{CeRh}_2\text{As}_2$  according to magnetic and thermodynamic bulk probes, showing the two superconducting phases SC1 and SC2 as well as the quadrupole-density-wave (QDW) phase. All measurements were conducted before this work, on the same batch of crystals (published in Refs. [4, 14], except the thermal expansion). The dashed lines highlight the ambiguity of the phase diagram: the QDW transition line may meet the superconducting region either at the multicritical point at  $\mu_0 H^* = 4\text{ T}$ , or at some higher field.

\*Corresponding author: konstantin.semeniuk@cpfs.mpg.de

†Corresponding author: elena.hassinger@tu-dresden.de

‡Corresponding author: manuel.brando@cpfs.mpg.de

face (FS) [1, 4, 15]. This model is based on a scenario proposed a decade ago for layered structures comprising loosely coupled layers of spin-singlet superconductors, with the sign of Rashba spin-orbit coupling alternating from layer to layer. Such systems were predicted to exhibit a SC phase diagram very similar to that observed in  $\text{CeRh}_2\text{As}_2$  [15–22]. Within this scenario, the transition between SC1 and SC2 was interpreted as a first order phase transition from an even- to an odd-parity SC order parameter [4], which in the case of  $\text{CeRh}_2\text{As}_2$  is also corroborated by the angle dependence of the SC upper critical field [14].

However, a quick look at Fig. 1 immediately poses a fundamental problem: The second order QDW phase boundary curves towards lower temperature with increasing field and seems to vanish near the endpoint of the first order line between the SC1 and SC2 phases. This strongly hints at a possibility of all four phase boundaries meeting at the same point, and the first order transition at  $H^*$  taking place between a mixed SC+QDW state (SC1) and a pure SC state (SC2) and not between an even- and an odd-parity order parameter. The scenario where the QDW order is responsible for the SC1-SC2 transition was considered in Refs. [4, 14], and was newly revisited in Ref. [23], where the QDW transition line could only be tracked until  $\mu_0 H \approx 4$  T. Besides that, a magnetic transition within the SC phase has been proposed as yet another interpretation of the  $H^*$  signature [24], resembling the case of high-pressure  $\text{CeSb}_2$  [25].

In our experiments so far, insufficient sample homogeneity and broadening of features in magnetic field prevented us from reliably tracking the QDW phase boundary close to the multicritical point. As illustrated in Fig. 1, large scatter of the  $T_0$  points leaves an ambiguity regarding the value of  $H$  at which the  $T_0(H)$  and  $T_c(H)$  lines meet. Progress on this front therefore demands samples of higher quality.

Here, we report a detailed study of specific heat and electrical resistivity of higher quality single crystals of  $\text{CeRh}_2\text{As}_2$  with  $T_c = 0.31$  K and  $T_0 = 0.48$  K, which exhibit much clearer signatures of the phase transitions. From these, we produce a more detailed  $T$ - $H$  phase diagram of  $\text{CeRh}_2\text{As}_2$  and demonstrate that the QDW phase boundary line meets the  $T_c(H)$  line at around 6 T — a significantly larger field than  $H^*$ . At the same time, we do not observe any signatures of  $T_0$  above 6 T within the SC2 phase, yet sudden disappearance of the QDW state at the SC2 phase boundary would go against thermodynamic principles.

A significant improvement of sample quality is illustrated with the help of Fig. 2, where thermodynamic and charge transport signatures of  $T_0$  and  $T_c$  are compared for the batch of  $\text{CeRh}_2\text{As}_2$  used in Refs. [1, 4, 14, 26] (old batch) and the new generation of samples studied in this work (new batch). One can identify two specific heat anomalies—the larger jump due to the SC transition and the smaller one due to the QDW instability—both of which appear as typical second-order phase transitions,

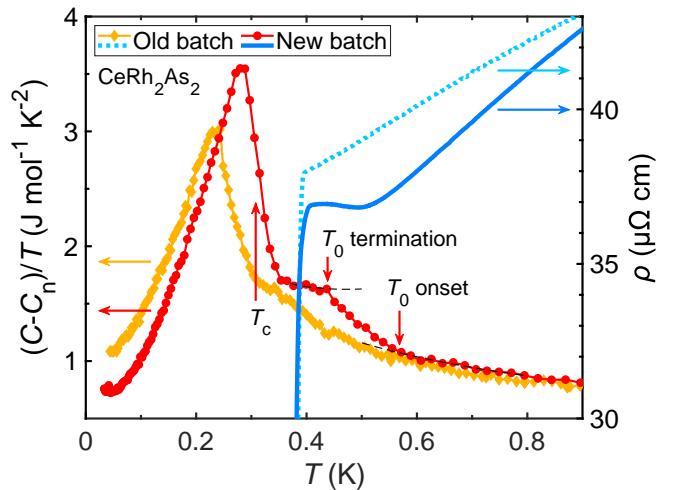


FIG. 2: Specific heat coefficient  $C(T)/T$  and resistivity  $\rho(T)$  of  $\text{CeRh}_2\text{As}_2$  as functions of temperature  $T$  showing signatures of the superconductivity and quadrupole-density-wave (QDW) instability ( $T_c$  and  $T_0$ , respectively) for two different generations of samples ("Old batch" denotes the samples used in Refs. [1, 4, 14], while samples from the "New batch" were used in this work). The dashed black lines extrapolate sections of  $C(T)/T$  for emphasizing the QDW transition. The specific heat is plotted after subtracting the nuclear contribution  $C_n(T)$  due to As atoms (detailed in the Supplemental Material). Resistivity of the old batch sample is scaled by a factor of 0.6.

affected by broadening. Samples of the new batch show a higher bulk  $T_c$  (0.31 K against 0.26 K) with a much sharper peak in specific heat  $C(T)$ , indicating a substantially improved homogeneity of crystals. The height of the jump at  $T_c$  is  $\Delta C/C|_{T_c} \approx 1.3$ , while the value of 1 was reported for the old samples [4]. The Sommerfeld coefficient  $\gamma = C/T$  for  $T \rightarrow 0$  decreases to  $0.7 \text{ J mol}^{-1} \text{ K}^{-2}$  in the new sample, which is a 40% reduction compared to the previous value of about  $1.2 \text{ J mol}^{-1} \text{ K}^{-2}$  [4], signifying a particularly strong sensitivity of superconductivity to disorder. The QDW transition is likewise more pronounced, with its onset and termination clearly visible as changes in the slope of  $C(T)/T$ . The strong increase of  $T_0$  from 0.4 K to 0.48 K with increasing sample quality is consistent with an itinerant nature of a sign changing order in  $k$ -space such as the proposed quadrupole density wave.

Since electrical resistivity is typically dominated by the most conductive part of the sample, the value of  $T_c$  corresponding to the resistivity drop can be regarded as an approximate upper bound for a distribution of  $T_c$  across a sample and is therefore higher than the thermodynamic counterpart. This discrepancy reflects the inhomogeneity of samples, also seen in other heavy-fermion systems [27]. It is therefore not surprising that the resistive  $T_c$  of 0.38 K measured for the new batch of  $\text{CeRh}_2\text{As}_2$  is not different from that of the old batch [1, 4]. What is

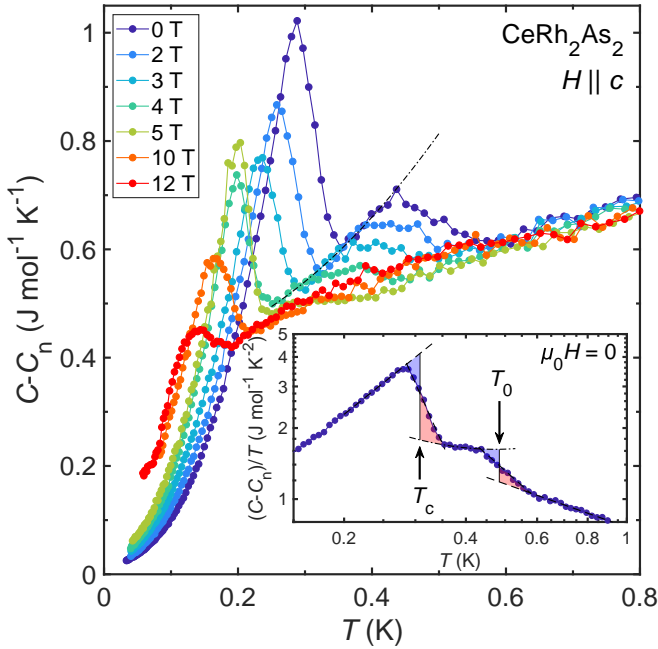


FIG. 3: Temperature dependence of the electronic specific heat  $C - C_n$  of  $\text{CeRh}_2\text{As}_2$  (new batch) measured at different  $c$ -axis magnetic fields. The inset shows the zero-field specific heat with the equal entropy construction used for defining the SC and QDW transition temperatures ( $T_c$  and  $T_0$ , respectively). The dash-dot line in both plots marks the envelope curve of  $C - C_n$  between the onset of  $T_c$  and the termination of  $T_0$ .

more remarkable, is that the higher  $T_0$  in the new batch makes the corresponding transport signature (resistivity upturn) much more apparent. Measurements of  $\rho(T)$  can therefore be used as a complementary technique for tracing the boundary of the QDW phase, which was rather challenging previously, as the transition at  $T_0$  got rapidly obscured by the resistivity drop at  $T_c$  upon applying field. The residual resistivity ratio (RRR) of the samples from the old batch is approximately 1.3, whereas for the new batch it reaches 2.8.

The low-temperature specific heat of  $\text{CeRh}_2\text{As}_2$  at different  $c$ -axis magnetic fields is shown in Fig. 3 (an extended set of data is provided in the Supplemental Material (SM) found below). Besides the pronounced peaks at  $T_c$  and  $T_0$ , there are no visible signatures of other phase transitions. Therefore, existence of the AFM order inside the SC phase [13] would imply that  $T_c = T_N$ , at least for  $H < H^*$ . Both  $T_c$  and  $T_0$  anomalies shift to lower temperatures upon applying magnetic field, with the  $T_0$  signature no longer apparent above 5 T.

In order to rigorously define and track  $T_c$  and  $T_0$  at different fields we used the equal entropy construction, shown in the inset of Fig. 3. For a given transition, the critical temperature was defined as the temperature at which the entropy change for a hypothetical zero-width transition was the same as the observed entropy change

for the real impurity-broadened transition. As visualized in the inset of Fig. 3, this corresponds to finding such values of  $T_c$  or  $T_0$  that equalize the integrals corresponding to the pink and purple shaded areas. For this analysis, we used the dash-dot line in Fig. 3 for extrapolating the specific heat in the QDW state at all relevant fields.

It is worth mentioning that the height of the specific heat jump at  $T_c$  exhibits a sharp increase as a function of field in a small interval around 4 T because of the kink in the SC phase boundary line at the multicritical point at  $H^*$  (as discussed in Ref. [4] and demonstrated in the SM). It is also instructive to look at the evolution of specific heat for  $5 \text{ T} \leq \mu_0 H \leq 7 \text{ T}$ , shown in Fig. 4. In this field range,  $T_c$  is nearly constant. The QDW transition is complete before the onset of superconductivity at 5 T, is interrupted at 6 T, and fully vanishes at 7 T. At the same time, the peak value of specific heat at  $T_c$  remains constant with respect to the unordered state ( $T > T_0$ ). Disappearance of the  $T_0$  signature between 5 T and 6 T is accompanied by a slight increase of specific heat below  $T_c$ .

In order to further verify the behavior of the QDW and SC phases in field, we measured electrical resistivity for current parallel to the basal plane of the  $\text{CeRh}_2\text{As}_2$  lattice and field along the  $c$  axis. The resultant data for selected fields are shown in Fig. 5, the extended set of data is available in the SM. The QDW transition is identifiable as a pronounced upturn in  $\rho(T)$  below  $\sim 0.6 \text{ K}$ , possibly due to a partial gapping of the FS [1]. In zero field, upon subsequent cooling, the upturn is followed by a downturn and the eventual SC transition, as detailed in the inset of Fig. 5. We defined  $T_0$  as the point of maximum curvature of  $\rho(T)$  (red dot), interpreting this

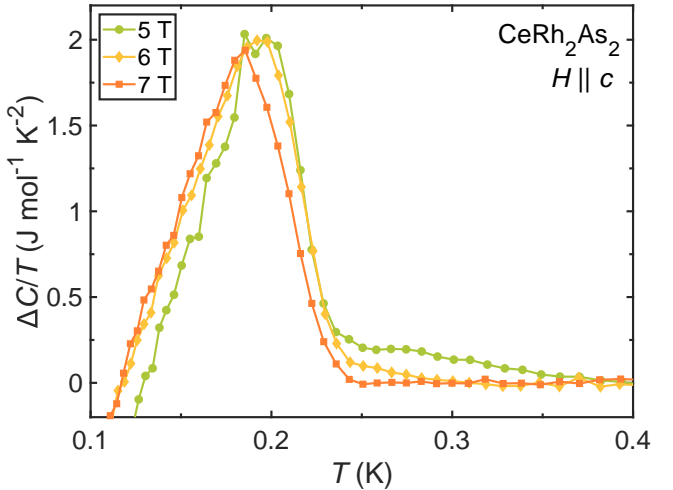


FIG. 4: Specific heat  $C(T)/T$  of  $\text{CeRh}_2\text{As}_2$  as a function of temperature  $T$  at selected values of  $c$ -axis magnetic field. The extrapolated unordered state specific heat was subtracted to emphasize the anomalies. For 5 T, a plateau between 0.25 K and 0.28 K indicates that the quadrupole-density-wave transition is complete before the superconductivity sets in.

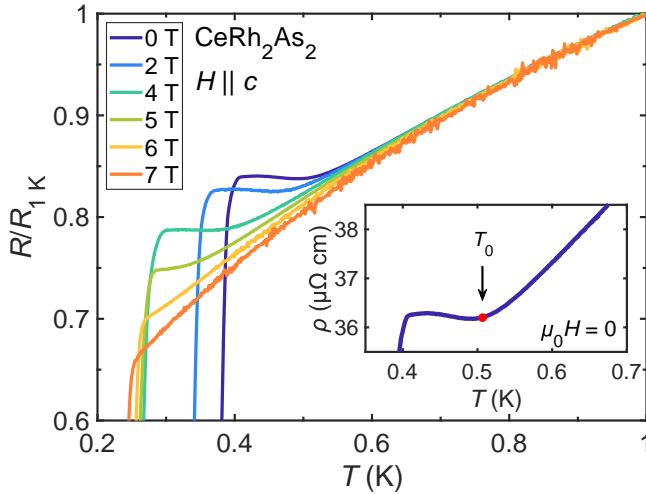


FIG. 5: Electrical resistance  $R$  against temperature  $T$  for  $\text{CeRh}_2\text{As}_2$  samples of the new batch, normalized to the resistance at 1 K, for different  $c$ -axis magnetic fields. Inset: zero-field resistivity  $\rho(T)$  in the vicinity of the quadrupole-density-wave instability. The transition temperature  $T_0$  was defined as the point of largest curvature (red dot).

temperature as the one at which the rate of charge carrier depletion on cooling is the highest (see the SM for details on determining  $T_0$ ). The resultant QDW phase boundary decently reproduces that obtained from specific heat measurements, as will be shown next.

We now discuss the  $T$ - $H$  phase diagram of  $\text{CeRh}_2\text{As}_2$  shown in Fig. 6. It summarizes the results of our specific heat and resistivity measurements conducted on samples from the new batch. First of all, the general shape of all phases—QDW, SC1, and SC2—is consistent with the previously published data [4, 23]. Remarkably, although the transition temperatures are generally higher than those shown by earlier generations of samples, the critical field  $\mu_0 H^*$  between SC1 and SC2 remains unchanged at 4 T. The zero-temperature limit of the SC upper critical field extrapolates to roughly 15 T and 18 T for specific heat and resistivity, respectively. Thanks to sharper transitions we can clearly identify  $T_0$  at fields as high as 5 T, which was not possible in previous studies (see Fig. 1). As shown in Fig. 4, it is even possible to see the onset of the QDW transition at 6 T, although the equal entropy principle could not be applied in this case. The  $T_0(H)$  line intercepts the SC2 phase boundary at approximately 6 T. Consequently, we can definitively conclude that the QDW phase boundary does not meet the multicritical point at  $\mu_0 H^* = 4$  T and is not responsible for the associated first order phase transition. Therefore, the point where the SC1 and SC2 phase boundaries meet is a bicritical one (indicated by the letter 'b' in Fig. 6).

According to thermodynamic considerations [28], it is not possible to have a multicritical point at some field  $H_c$ , such that two second order phase boundaries come out of it for  $H < H_c$  and one phase boundary (first or

second order) comes out for  $H > H_c$  (holds true if the inequalities are swapped). Applied to the crossing of the SC and QDW phase boundaries at 6 T, this constraint requires that the  $T_0(H)$  line continues inside the SC2 state, resulting in a tetracritical point (indicated by the letter 't' in Fig. 6), assuming that the QDW transition remains of the second order below  $T_c$ . That said, we do not observe any signature of the QDW instability within the SC2 phase (cf. 7 T curve in Fig. 4). Given the steep slope of the  $T_0(H)$  line near 6 T, it is quite possible that the transition evaded detection due to being too broad or the field sampling period of 1 T being too large.

It is therefore worth analyzing the experimental phase diagram in terms of the Ginzburg-Landau (GL) theory of coupled order parameters [29], as done, e.g., for iron pnictide superconductors in Ref. [30]. The coupling term in the free energy between the SC2 and QDW order parameters,  $\Delta$  and  $\mathbf{Q}$  respectively, is given by  $\lambda\Delta^2\mathbf{Q}^2$ , where  $\lambda$  indicates the strength of the coupling as well as its nature,  $\lambda > 0$  for competing and  $\lambda < 0$  for supporting coupling. We reproduced our experimental phase diagram by using the values of the transition temperatures, the slopes of the phase boundary lines and most importantly the jumps of the specific heat coefficients at the transition temperatures,  $\Delta C(T_0)/T_0$  and  $\Delta C(T_c)/T_c$ , which are directly related to the condensation energies and to

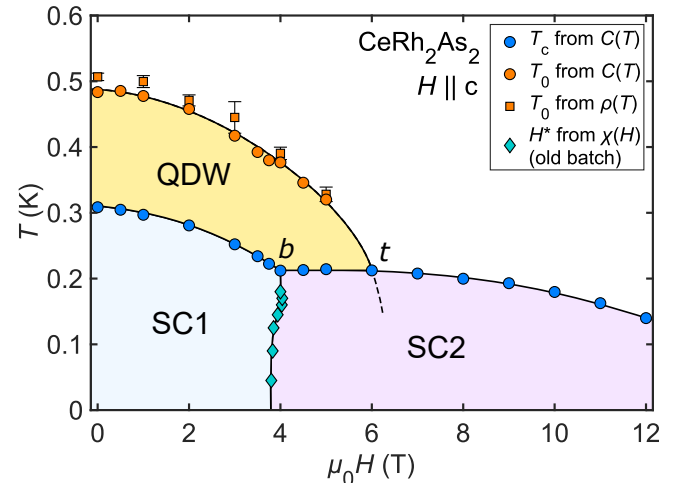


FIG. 6: Temperature -  $c$ -axis magnetic field ( $T$ - $H$ ) phase diagram of  $\text{CeRh}_2\text{As}_2$  depicting the two superconducting (SC) phases SC1 and SC2 as well as the quadrupole-density-wave (QDW) phase. The SC and QDW transition temperatures ( $T_c$  and  $T_0$ , respectively) were obtained from measurements of specific heat  $C(T)$  and electrical resistivity  $\rho(T)$  conducted on samples from the new batch. The SC1-SC2 first order phase boundary, terminating in a bicritical point  $b$ , is plotted according to earlier AC magnetic susceptibility  $\chi(H)$  data [4]. The solid black lines are guides for the eye. The dashed line marks a segment of a so far undetected hypothetical phase boundary expected from thermodynamic considerations, while  $t$  marks the corresponding tetracritical point.

the changes in the slopes of the  $T_0(H)$  and  $T_c(H)$  lines at  $t$ . A detailed analysis is provided in the SM and visualised with the help of Fig. S8; here we summarize the main findings: i) The absence of a pronounced kink in the  $T_c(H)$  line while crossing the  $t$  point at 6 T, together with the presence of three second order phase lines escaping  $t$  and no signatures of a first order line ending at  $t$  in this and previous experiments [4], definitely imply that the coupling between the QDW and SC2 order parameters is not strong. A strong competition would result in a bi-critical point, with an emerging first order line extending down to  $T = 0$  (Fig. S8c). ii) A negative  $\lambda$  (supporting coupling) is also unlikely, since it flattens the  $T_0(H)$  line below  $t$  (Fig. S8d), and we should have then observed a double feature in  $C(T)/T$  at 7 T. iii) Interestingly, for a weak  $\lambda$ , the slope change across  $t$  would be substantial for the  $T_0(H)$  line (Fig. S8a), but not for the  $T_c(H)$  line, with a difference of about two orders of magnitude. This is due to the fact that the changes of the slopes at  $t$  are related to  $\Delta C(T_0)/T_0$  and  $\Delta C(T_c)/T_c$  evaluated at  $t$ . Extrapolating the steps in  $C/T$  at  $T_c(H)$  and  $T_0(H)$  from  $H > H_t$  and  $H < H_t$ , respectively, to  $H = H_t$ , one gets  $\Delta C(T_0)/T_0 \approx \frac{1}{10} \Delta C(T_c)/T_c$ . As a concrete example, a change in the slope of the  $T_0(H)$  line caused by a weak coupling—about 20% of the strength necessary to induce a first order transition—would shift the critical field of the QDW phase at  $T = 0$  down by about 0.4 T compared to the case of no coupling, resulting in no QDW-related feature observable in specific heat at 7 T. At the same time,  $T_c$  should slightly increase between the  $b$  and  $t$  points. The phase below the line joining  $b$  and  $t$  is a phase in which the two states homogeneously coexist [30]. We actually observe a slight change in the slope of  $T_c(H)$  at  $t$  (see Fig. S9 of the SM), consistent with the weak coupling scenario, but extraction of quantitative information is hindered by the insufficient resolution of our data.

In iron pnictide superconductors, it is known that the same electrons are responsible for both the magnetic ordering as well as the superconductivity, and an analysis with the GL theory is appropriate. In the case of  $\text{CeRh}_2\text{As}_2$ , the situation is more complex due to the presence of two relevant sheets of the FS. To gauge the degree of interplay expected between the QDW and SC2 states we consider the electronic structure of  $\text{CeRh}_2\text{As}_2$ . The FS predicted by the most reliable renormalized band structure calculations so far [1] contains a quasi-three-dimensional strongly-corrugated cylinder (3D-sheet) along the  $\Gamma$ - $Z$  direction of the Brillouin zone (BZ) and quasi-two-dimensional corrugated cylinders (2D-sheet) along axes parallel to the  $A$ - $M$  direction. Within the parity change picture of the SC1-SC2 transition, the SC pairing is mainly driven by the electrons of the 2D-sheet, located at the edges of the BZ, where the spin-orbit coupling dominates over the interlayer hopping [15]. A recent study [23] demonstrated that the upturn of  $\rho(T)$  at  $T_0$  is stronger when the current flows along the  $c$  axis as opposed to the  $ab$  plane, mean-

ing that the associated FS nesting vector must have a sizeable out-of-plane component, rather than be pointed strictly in the in-plane direction [1]. The states involved in the QDW instability are therefore expected to belong to the 3D-sheet of the FS. The attribution of the two orders to the different FS sheets disfavours a strong coupling between the QDW and superconductivity, and one would then expect the  $T_0(H)$  line to continue into the SC2 phase practically undisturbed.

To conclude, using new higher quality crystals we refined the  $T$ - $H$  phase diagram of  $\text{CeRh}_2\text{As}_2$  for field parallel to the  $c$  axis. Our data unambiguously demonstrate that the QDW phase boundary does not meet the bi-critical point located between the two SC phases and is therefore not responsible for the first order phase transition between SC1 and SC2. The  $T_0(H)$  line intercepts the SC2 phase boundary at a tetracritical point near 6 T. From the analysis of the phase boundary lines near the tetracritical point we deduce that there is a weak competing interaction between the SC and QDW order parameters. These conclusions leave us with two viable explanations for the origin of the transition between SC1 and SC2: the even-to-odd parity switching [4, 14] or a change in magnetic ordering [24]. Our results prompt a further study of the 6 T tetracritical point, from which an additional phase boundary is expected to emerge.

## Acknowledgments

We are indebted to D. Agterberg, D. Aoki, S. Kitagawa, G. Knebel, K. Ishida, A. P. Mackenzie, A. Rost, O. Stockert, Y. Yanase and G. Zwicknagl for useful discussions. This work was supported by the joint Agence National de la Recherche and DFG program Fermi-NESt through Grants No. GE602/4-1 (C. G. and E. H.). Additionally, E. H. acknowledges funding by the DFG through CRC1143 (project number 247310070) and the Würzburg-Dresden Cluster of Excellence on Complexity and Topology in Quantum Matter — ct.qmat (EXC 2147, project ID 390858490).

## Supplemental Material

### I. SUBTRACTION OF NUCLEAR CONTRIBUTION TO HEAT CAPACITY

Here we evaluate the Schottky nuclear contribution to the specific heat of  $\text{CeRh}_2\text{As}_2$ . Since Ce has no nuclear moment and the contribution from the Rh nuclear moment is well below 1 mK [31, 32], the only relevant contribution to the specific heat is from the  $^{75}\text{As}$  nuclear moment  $I = 3/2$  (100% abundance).  $\text{CeRh}_2\text{As}_2$  has a tetragonal structure with two sites for the As atoms, As(1) and As(2). Similar analysis was done by Hagino *et al.* for  $\text{CuV}_2\text{S}_4$  (Cu nuclear spin  $I = 3/2$ ) [33].

The nuclear-spin Hamiltonian of an atomic nucleus with a spin quantum number  $I$  and a magnetic moment  $\mu_I = g_N \mu_N I$  with  $\mu_N = 5.05 \times 10^{-27} \text{ J/T}$  (nuclear magneton) and  $g_N$ , the nuclear  $g$ -factor, consists of the sum of quadrupolar and Zeeman terms:

$$H = \frac{e^2 q Q}{4I(2I-1)} \left[ 3m_I^2 - I(I+1) + \frac{1}{2}\eta(I_+^2 + I_-^2) \right] - \gamma_N \hbar I \cdot B \quad (\text{S1})$$

where  $\gamma_N = g_N \mu_N / \hbar$  is the gyromagnetic ratio,  $\eta$  is the anisotropy parameter, and  $m_I$  is the azimuthal quantum number with allowed values  $I, I-1, \dots, -I$ . The equally spaced energy levels in an effective field  $B_{\text{eff}}$  are:

$$\varepsilon_m = -\mu_I \cdot B_{\text{eff}} = -g_N \mu_N m_I B_{\text{eff}} \quad (\text{S2})$$

so the energy difference between the  $2I+1$  levels is:

$$\Delta\varepsilon = -g_N \mu_N B_{\text{eff}}. \quad (\text{S3})$$

This energy gap is generally very small and the Schottky peaks usually occur at temperatures of the order of mK; consequently, in the temperature range of our measurements only the high-temperature part of the peak can be observed and the analysis can be made using only the proportional factor  $\alpha = C_n T^2$  which can be written as:

$$\alpha = \frac{R}{3} I(I+1) \left( \frac{\hbar \gamma_N}{k_B} \right)^2 B_{\text{eff}}^2 \quad (\text{S4})$$

where  $\gamma_N = \omega_N / B_{\text{eff}}$  corresponds to an NMR-frequency  $\omega_N$  which gives an energy splitting of  $\hbar\omega_N$  in an effective magnetic field  $B_{\text{eff}}$ . It can be calculated/measured for every isotope and is of the order of  $10^6 \text{ Hz/T}$ .

If a nucleus has a quadrupole moment  $Q$  ( $I \geq 3/2$ ) and is situated in a non-spherical or non-cubic electronic environment, its interaction with the field gradient  $V_{zz} = eq$  (for an axially symmetric field gradient  $\eta = 0$ ) produced by neighboring atoms will cause small splittings of the energy levels:

$$\Delta\varepsilon = \varepsilon(m_I) - \varepsilon(m'_I) = \frac{3e^2 q Q}{4I(2I-1)} |m_I^2 - m'^2_I| \quad (\text{S5})$$

TABLE I: The  $^{75}\text{As}$  atom.

Parameters	Constants
$I = 3/2$	$k_B = 1.38 \times 10^{-23} \text{ J/K}$
$Q = 0.3 \times 10^{-28} \text{ m}^2$	$e = 1.6 \times 10^{-19} \text{ C}$
$\gamma = 7.294 \text{ MHz/T}$	$h = 6.63 \times 10^{-34} \text{ Js}$
Abundance = 100%	$R = 8.31 \text{ J/Kmol}$

and the proportional factor in the Schottky specific heat can be given by

$$\alpha = \frac{R}{80} \left( \frac{e^2 q Q}{k_B} \right)^2 \frac{(I+1)(2I+3)}{I(2I-1)}. \quad (\text{S6})$$

In zero magnetic field, the energy difference given by Eq. S5 is:

$$\Delta = \frac{1}{2} e^2 q Q \quad (\text{S7})$$

which corresponds to an NQR frequency  $\nu_Q = \Delta/h$ .

The  $^{75}\text{As}$  level scheme is shown in Fig. S1 and all relevant parameters are listed in Tab. I.

The energy levels  $\epsilon_i$  can be calculated:

$$\begin{aligned} \epsilon_1 &= -\frac{\Delta}{2} - \frac{1}{2} \gamma_N \sqrt{4 - 3 \cos^2(\theta)} \\ \epsilon_2 &= -\frac{\Delta}{2} + \frac{1}{2} \gamma_N \sqrt{4 - 3 \cos^2(\theta)} \\ \epsilon_3 &= +\frac{\Delta}{2} - \frac{3}{2} \gamma_N \cos(\theta) \\ \epsilon_4 &= +\frac{\Delta}{2} + \frac{3}{2} \gamma_N \cos(\theta) \end{aligned}$$

and the high-temperature part of the Schottky molar heat capacity that we can observe in the experiment is:

$$\alpha = C_n T^2 = \frac{R}{4} \left( \frac{\Delta}{k_B} \right)^2 = R \left( \frac{e^2 q Q}{4k_B} \right)^2. \quad (\text{S8})$$

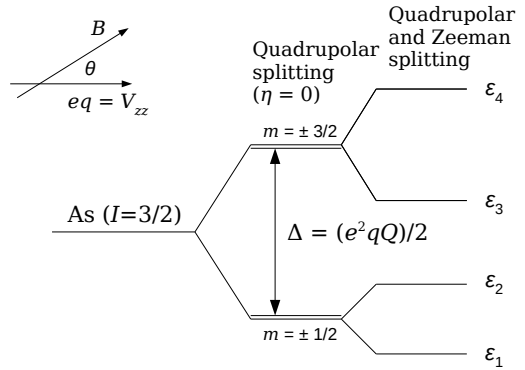


FIG. S1: The nuclear quadrupole splitting and the Zeeman splitting for the  $^{75}\text{As}$  nuclear spin  $I$  with and without magnetic field  $B$ . The field gradient  $eq = V_{zz}$  is axially symmetric ( $\eta = 0$ ).

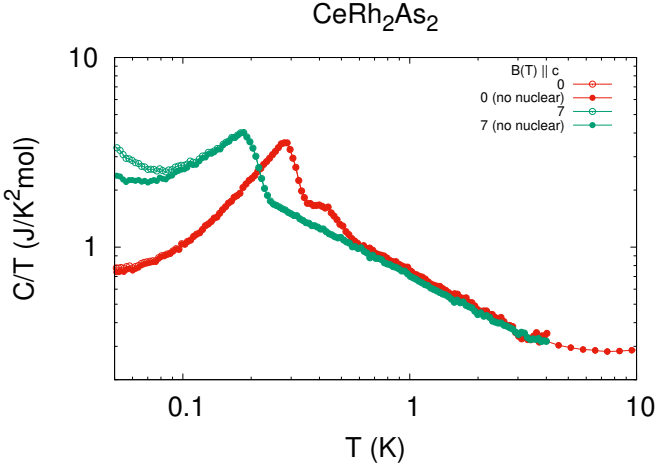


FIG. S2: Specific heat plotted for  $B = 0$  and  $7\text{ T}$  with and without nuclear contribution.

In magnetic field  $B$  with  $\theta = 0$  it becomes:

$$\alpha(B) = C_n(B)T^2 = \frac{5R}{4} \left( \frac{\gamma_N \hbar B}{k_B} \right)^2. \quad (\text{S9})$$

We can now use the measured NQR frequencies from Kibune *et al.* [13] to calculate the energy splittings:

As(1) :

$$\nu_Q = \Delta/h = 31.1 \text{ MHz}$$

$$\Delta = 2.06 \times 10^{-26} \text{ J} = 1.49 \text{ mK}$$

As(2) :

$$\nu_Q = \Delta/h = 10.75 \text{ MHz}$$

$$\Delta = 0.71 \times 10^{-26} \text{ J} = 0.51 \text{ mK}.$$

Considering that the values for the energy splittings are very low (about 1 mK), a very small contribution to the specific heat should be observed at temperatures between 50 mK and 100 mK in zero field, as shown in Fig. S2.

From these data we calculate the  $\alpha$  coefficient using Eq. S8:

$$\text{As(1)} : \alpha = 4.63 \times 10^{-6} \text{ J K/mol}$$

$$\text{As(2)} : \alpha = 0.55 \times 10^{-6} \text{ J K/mol}$$

$$\text{Total value} : \alpha = 5.18 \times 10^{-6} \text{ J K/mol}$$

In magnetic field we can use the NMR frequency  $\gamma_N = 2\pi\gamma = 45.8 \text{ MHz/T}$ , and with Eq. S9 we obtain:

$$\text{Total-value} : \alpha(B) = 2.54 \times 10^{-6} \times B^2 \text{ JK mol}^{-1} \text{ T}^{-2}.$$

## II. EXTENDED HEAT CAPACITY DATA SET

In Fig. S3 we show the raw data of specific heat of  $\text{CeRh}_2\text{As}_2$  down to 40 mK, for  $c$ -axis magnetic fields of up to 12 T, with steps of 1 T.

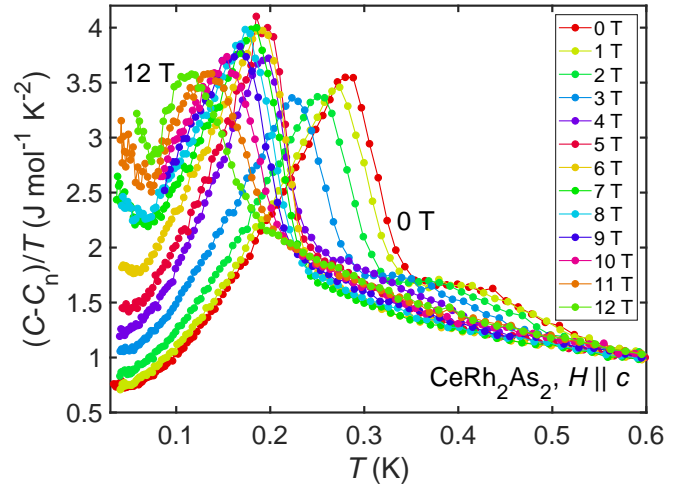


FIG. S3: Temperature dependence of electronic specific heat  $(C - C_n)/T$  of  $\text{CeRh}_2\text{As}_2$  at different magnetic fields applied along the  $c$ -axis.

## III. FIELD DEPENDENCE OF THE SPECIFIC HEAT JUMP AT THE SUPERCONDUCTING TRANSITION

Applying the equal entropy construction (described in the main paper) allowed us to determine the ideal specific heat jump heights  $\Delta C/T$  at  $T_c$  for different  $c$ -axis magnetic fields. In Fig. S4 we plot the field dependence of the  $C/T$  jump at  $T_c$ . The jump height increases suddenly as the field crosses the  $\mu_0 H^* = 4 \text{ T}$  value. This change is linked to the existence of the first order SC1-SC2 phase boundary at 4 T [28]. At 6 T, the two transitions overlap, hindering the equal entropy analysis. For this particular point, we provide the  $C/T$  jump height with respect to

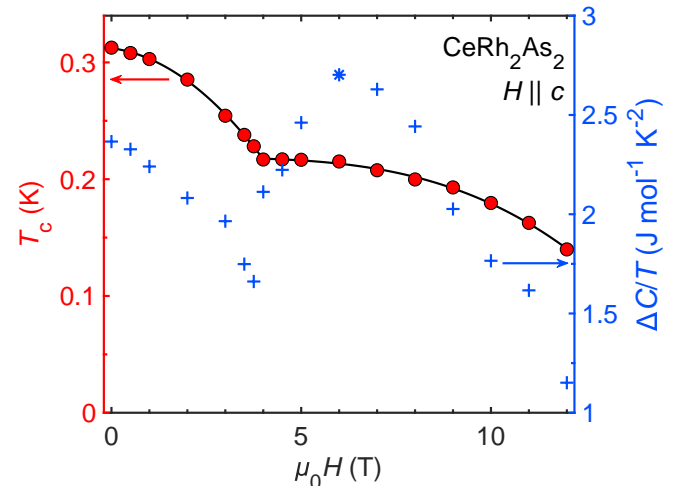


FIG. S4: Left axis:  $c$ -axis magnetic field dependence of  $T_c$ , according to the heat capacity data. Right axis: the ideal specific heat  $(C/T)$  jump at  $T_c$ .

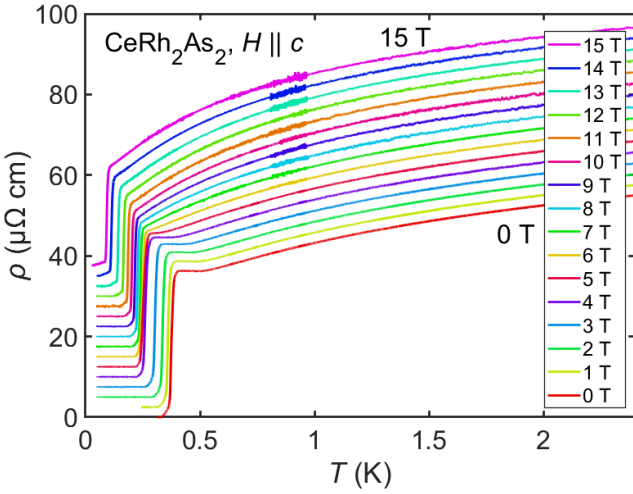


FIG. S5: Resistivity ( $\rho$ ) of  $\text{CeRh}_2\text{As}_2$  as a function of temperature ( $T$ ) at different  $c$ -axis magnetic fields. The curves are offset from each other by  $2.5 \mu\Omega \text{ cm}$  for improved clarity.

the extrapolated unordered state (the state above the onset of the QDW transition). Since we observe the onset of the QDW transition at  $6 \text{ T}$ , the plotted value (\* marker) overestimates the actual ideal  $C/T$  jump height at the SC transition.

#### IV. EXTENDED RESISTIVITY DATA SET

In Fig. S5 we show the raw data of electrical resistivity of  $\text{CeRh}_2\text{As}_2$  between  $50 \text{ mK}$  and  $2 \text{ K}$  for  $c$ -axis magnetic fields of up to  $15 \text{ T}$ , with steps of  $1 \text{ T}$ .

#### V. DETERMINATION OF $T_0$ FROM RESISTIVITY

Resistivity upturn is a common signature of density-wave type transitions (e.g. Ref. [34]). When it occurs at temperatures well above  $1 \text{ K}$ , the transition generally appears as a kink of negligible width compared to the temperature interval of interest. In our case, the transition takes place over significant portions of temperature sweeps, and deciding which particular temperature value to take as  $T_0$  becomes non-trivial.

We interpret the resistivity upturn as a partial gapping of the Fermi surface. It is therefore sensible to define the midpoint of the QDW transition as the point where the curvature of  $\rho(T)$ , i.e. its second derivative, is the largest. This value of  $T_0$  can be vaguely interpreted as the temperature at which the rate of charge carrier depletion is the highest. Numerical differentiation of  $\rho(T)$  using the finite difference method produces excessively noisy data. Instead, we determined the second derivative using the Savitzky-Golay smoothing procedure (the result is summarised in Fig. S6). Before processing a sweep, we first

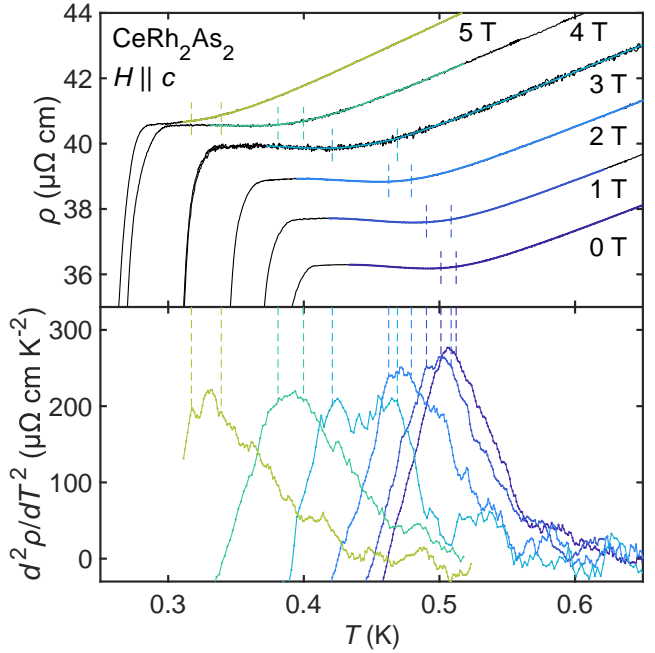


FIG. S6: Determination of the QDW transition temperature  $T_0$  according to measurements of resistivity  $\rho(T)$ . Top: raw resistivity (black curves) with smoothed data plotted on top for different  $c$ -axis magnetic fields. The curves are offset by  $1.5 \mu\Omega \text{ cm}$ . Bottom: second derivatives of resistivity with respect to temperature. The vertical dashed lines mark the upper and lower bounds for locating the second derivative maxima. The smoothing and differentiation procedures are explained in the text.

truncated it just above the onset of superconductivity, to ensure that we considered only the normal state resistivity. We then binned the  $\rho(T)$  data into intervals of  $1 \text{ mK}$  ( $0 \text{ T}$ ,  $1 \text{ T}$ ,  $2 \text{ T}$ ,  $5 \text{ T}$  sweeps) or  $2 \text{ mK}$  ( $3 \text{ T}$ ,  $4 \text{ T}$  sweeps), which were slightly more noisy and calculated the mean value for each bin, thus obtaining resistivity at regularly sampled temperatures. Next, we applied a second order Savitzky-Golay filter, which works by fitting a polynomial of the corresponding order to a moving window. The second derivative is given by the curvature of this smoothing polynomial (a parabola in our case). The width of the moving window was either  $50 \text{ mK}$  or  $60 \text{ mK}$  (the larger window was used for the  $3 \text{ T}$  and  $4 \text{ T}$  sweeps). We then visually estimated the temperature interval which was guaranteed to contain the peak of the second derivative. The center of that interval was taken as  $T_0$ , while its width defined the uncertainty.

#### VI. EXPANDED T-H PHASE DIAGRAM

In Fig. S7 we show the expanded version of the  $T$ - $H$  phase diagram of  $\text{CeRh}_2\text{As}_2$  depicted in Fig. 6 of the main paper. In this version we added the  $T_c$  values obtained from resistivity measurements. The associated er-

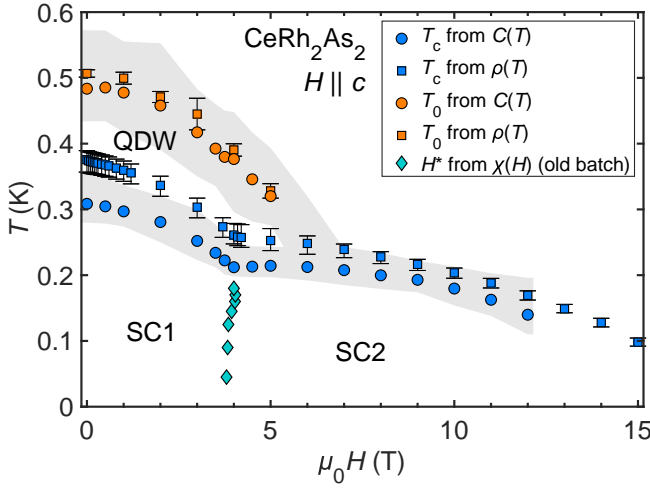


FIG. S7: The expanded version of the temperature -  $c$ -axis magnetic field ( $T$ - $H$ ) phase diagram of  $\text{CeRh}_2\text{As}_2$  shown in Fig. 6 of the main paper. Definitions of the additional quantities and error bars plotted are explained in the text.

rror bars represent the width of the SC transition, defined as the interval between the 5% and 95% resistivity drop thresholds. The light grey area marks the onset-to-termination intervals for the  $T_c$  and  $T_0$  transitions in specific heat.

## VII. GINZBURG-LANDAU THEORY OF COUPLED ORDER PARAMETERS

The interplay between the SC and QDW orders in  $\text{CeRh}_2\text{As}_2$  near the tetracritical point of the  $T$ - $H$  phase diagram (Fig. 6 of the main article) can be analyzed in terms of a Ginzburg-Landau (GL) theory of coupled order parameters [29, 30]. Considering spatially uniform order parameters for the two phases,  $\Delta$  (SC) and  $\mathbf{Q}$  (QDW), the free energy is given as:

$$F(\Delta, \mathbf{Q}) = \frac{a_1}{2} \Delta^2 + \frac{b_1}{4} \Delta^4 + \frac{a_2}{2} \mathbf{Q}^2 + \frac{b_2}{4} \mathbf{Q}^4 + \lambda \Delta^2 \mathbf{Q}^2 \quad (\text{S10})$$

where  $\lambda \Delta^2 \mathbf{Q}^2$  is the coupling term. For  $\lambda > 0$  the interaction is repulsive and represents competition between the two orders, while for  $\lambda < 0$  the interaction is attractive resulting in supporting coupling (one enhances the other).

We assume  $T$ -independent  $b_1, b_2 > 0$ , and close to the transition temperatures  $T_0$  and  $T_c$ , we expand

$$\begin{aligned} a_1(T) &= a_1(0)(T/T_c - 1) \\ a_2(T) &= a_2(0)(T/T_0 - 1). \end{aligned}$$

There are four solutions in zero field ( $H = 0$ ): the unordered state (i), the SC state (ii), the QDW state

(iii) and the mixed state (iv):

- i)  $(\Delta_0, Q_0) = (0, 0)$
- ii)  $(\Delta_0, Q_0) = (\pm \sqrt{-a_1/b_1}, 0)$
- iii)  $(\Delta_0, Q_0) = (0, \pm \sqrt{-a_2/b_2})$
- iv)  $(\Delta_0, Q_0) = \left( \pm \sqrt{\frac{a_1 b_2 - 2 a_2 \lambda}{4 \lambda^2 - b_1 b_2}}, \pm \sqrt{\frac{a_2 b_1 - 2 a_1 \lambda}{4 \lambda^2 - b_1 b_2}} \right)$

with condensation energies at  $H = 0$ :

$$\begin{aligned} i) \quad \Delta F &= 0 \\ ii) \quad \Delta F &= -\frac{a_1^2}{4b_1} \\ iii) \quad \Delta F &= -\frac{a_2^2}{4b_2} \\ iv) \quad \Delta F &= -\frac{a_1^2 b_2 - 4 a_1 a_2 \lambda + a_2^2 b_1}{4(b_1 b_2 - 4 \lambda^2)}. \end{aligned}$$

We can now use the experimental values of the transition temperatures ( $T_c$  ;  $T_0$ ) and the jumps in the specific heat coefficients at the transitions ( $A_c = \Delta C(T_c)/T_c$  ;  $A_0 = \Delta C(T_0)/T_0$ ) from the unruled state to the ordered states to calculate the parameters for every state independently. For instance, the specific heat change associated to the superconducting transition is

$$\Delta C(T_c) = \frac{a_1^2(0)}{2b_1 T_c}. \quad (\text{S11})$$

Assuming a power-law behavior for specific heat of the form  $C(T)/T = -\Delta\gamma + cT^n$  and inserting the magnetic field dependence as terms in the free energy as  $a_1(0) \left( \frac{H}{H_c(0)} \right)^m \Delta^2$  and  $a_2(0) \left( \frac{H}{H_0(0)} \right)^m \mathbf{Q}^2$ , it is possible to reproduce the experimental phase diagrams for the SC2 and QDW states of  $\text{CeRh}_2\text{As}_2$  without interaction ( $\lambda = 0$ ) and extract the  $n$  and  $m$  parameters. These are plotted in Fig. S8 for  $T_c = 0.22$  K and  $T_0 = 0.49$  K as red and blue lines, respectively.

By solving the GL equations with the coupling term and considering that at the 't' point ( $H_t, T_t$ ) of the phase diagram (Fig. 6 of the main article)  $T_c(H_t) = T_0(H_t)$ , one can draw the phase diagrams for different values of the coupling parameter  $\lambda$ . In fact, performing a similar calculation as in Ref. [30], one derives simple expressions for the field dependences of the transition temperatures:

$$T_c(H) = T_t \left[ 1 + \frac{f(H)}{1 - \frac{\Gamma}{2A_c(T_t)}} \right] \text{ for } H < H_t \quad (\text{S12})$$

$$T_0(H) = T_t \left[ 1 + \frac{f(H)}{1 - \frac{2A_0(T_t)}{\Gamma}} \right] \text{ for } H > H_t \quad (\text{S13})$$

where we assume  $T_0(H) = T_t[1 + f(H)]$  for  $H < H_t$ ,  $df(H)/dH < 0$ ,  $f(H_t) = 0$  and  $T_c$  independent of  $H$

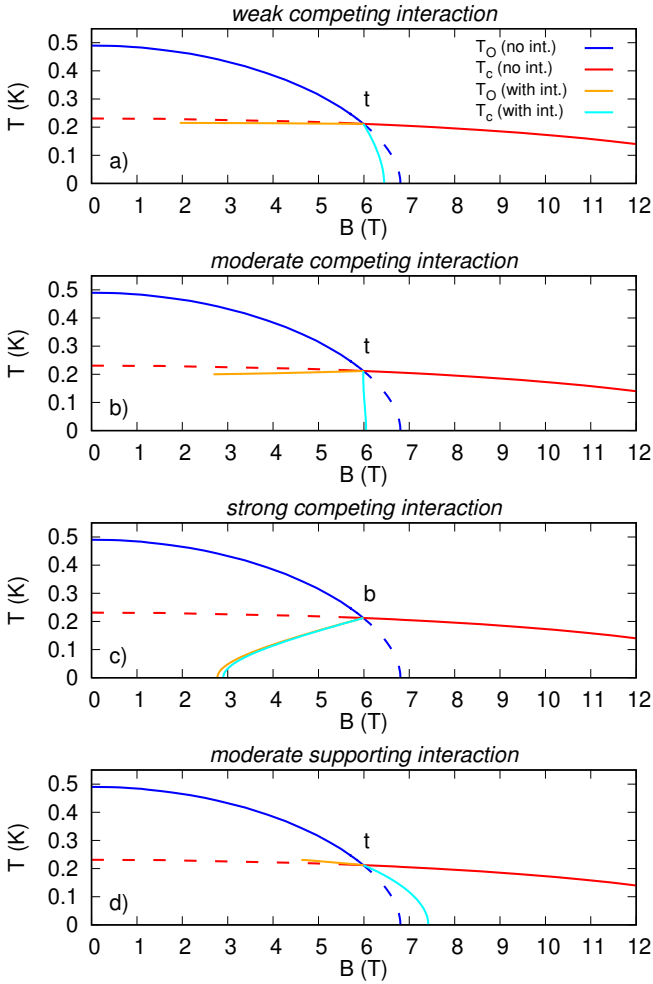


FIG. S8: Temperature-field ( $T$ - $B$ ) phase diagrams for different values of the coupling parameter  $\lambda$ .  $B = \mu_0 H$  in tesla. The value of  $\lambda$  for the weak coupling in panel a) is about 20% of the value necessary to induce a first order phase transition as shown in panel c). The letter 't' indicates the tetracritical point, whereas the letter 'b' indicates the bicritical point. The red and blue lines represent the phase boundaries without interaction (int.), with parts that get modified by the interaction drawn as dashed lines.

for  $H > H_t$ .  $\Gamma$  is the scaled interaction strength, corresponding to the interaction energy  $E_{\text{int.}} = \Gamma T_t^2$ , by analogy with the condensation energies of both phases being  $E_c = A_c T_t^2$  and  $E_0 = A_0 T_t^2$ . The phase boundary lines from these equations are plotted in Fig. S8 as orange and cyan lines.

We now describe the results starting from the panel a), i.e. weak coupling. By weak coupling we mean a value of  $\lambda$  which is 20% of that necessary to induce a first order phase transition (case shown in panel c)). We have four second order phase transition lines joining at  $t = (H_t, T_t)$ , the tetracritical point. Although the coupling is weak, a substantial change in slope of the  $T_0(H)$  line is observed

at  $t$  (blue to cyan line). The line becomes steeper, and with a moderate coupling (50% relative to the case in panel c)), it becomes almost vertical (shown in panel b)). This could explain why we do not observe this line in the experiments and why we do not detect any transition in specific heat at 7 T, in particular. In contrast, the phase boundary of the superconducting phase for  $H < H_t$  is not affected at all. This is due to the fact that the slope is proportional to the specific heat jumps  $A_c$  and  $A_0$  evaluated at  $t$  (cf. equations above), and we have  $\Delta C(T_0)/T_0 \approx \frac{1}{10} \Delta C(T_c)/T_c$  from the experiment.

A strong coupling is expected to induce a first order transition between the SC and QDW phases as shown by the merging orange and cyan lines in panel c) of Fig. S8. The joining point is therefore a bicritical point 'b'. This is definitely not the case in  $\text{CeRh}_2\text{As}_2$ .

Finally, a supporting interaction ( $\lambda < 0$ ) results in a flattening of the  $T_0(H)$  line upon crossing  $t$  (shown in panel d)), in which case the  $T_0$  transition should have been observed in our experiments at 7 T.

A careful look at our experimental data reveals what seems to be a small change in the slope of the  $T_c(H)$  line at about 6 T. As emphasized in Fig. S9,  $T_c$  remains more or less constant in the 4 T to 6 T range and clearly decreases with field for  $\mu_0 H > 6$  T. The resolution of our data is insufficient for a reliable determination of the slope change, but the observed behavior decently matches the one predicted for the weak competing coupling regime. We therefore propose that this particular case describes the interaction between the SC and QDW orders in  $\text{CeRh}_2\text{As}_2$ .

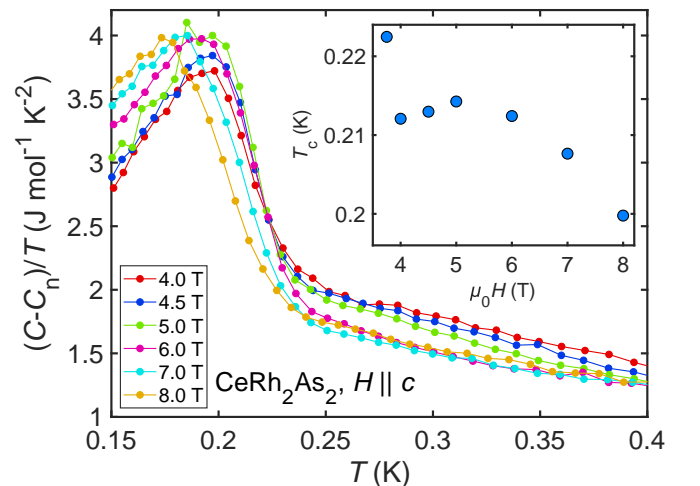


FIG. S9: Temperature ( $T$ ) dependence of electronic specific heat  $(C - C_n)/T$  of  $\text{CeRh}_2\text{As}_2$  at specific values of the  $c$ -axis magnetic field between 4 T and 8 T. Inset: field dependence of the superconducting transition temperature  $T_c$  in a similar field region.

---

[1] D. Hafner, P. Khanenko, E.-O. Eljaouhari, R. Küchler, J. Banda, N. Bannor, T. Lühmann, J. F. Landaeta, S. Mishra, I. Sheikin, et al., Phys. Rev. X **12**, 011023 (2022), URL <https://journals.aps.org/prx/abstract/10.1103/PhysRevX.12.011023>.

[2] J. Effantin, J. Rossat-Mignod, P. Burlet, H. Bartholin, S. Kunii, and T. Kasuya, J. Magn. Magn. Mater. **47-48**, 145 (1985), ISSN 0304-8853, URL [https://doi.org/10.1016/0304-8853\(85\)90382-8](https://doi.org/10.1016/0304-8853(85)90382-8).

[3] J. Kitagawa, N. Takeda, and M. Ishikawa, Phys. Rev. B **53**, 5101 (1996).

[4] S. Khim, J. F. Landaeta, J. Banda, N. Bannor, M. Brando, P. M. R. Brydon, D. Hafner, R. Küchler, R. Cardoso-Gil, U. Stockert, et al., Science **373**, 1012 (2021), URL <https://www.science.org/doi/10.1126/science.abe7518>.

[5] R. A. Fisher, S. Kim, B. F. Woodfield, N. E. Phillips, L. Taillefer, K. Hasselbach, J. Flouquet, A. L. Giorgi, and J. L. Smith, Phys. Rev. Lett. **62**, 1411 (1989), URL <https://journals.aps.org/prl/abstract/10.1103/PhysRevLett.62.1411>.

[6] G. Bruls, D. Weber, B. Wolf, P. Thalmeier, B. Lüthi, A. deVisser, and A. Menovsky, Phys. Rev. Lett. **65**, 2294 (1990), URL <https://journals.aps.org/prl/abstract/10.1103/PhysRevLett.65.2294>.

[7] S. Adenwalla, S. W. Lin, Q. Z. Ran, Z. Zhao, J. B. Ketterson, J. A. Sauls, L. Taillefer, D. G. Hinks, M. Levy, and B. K. Sarma, Phys. Rev. Lett. **65**, 2298 (1990), URL <https://journals.aps.org/prl/abstract/10.1103/PhysRevLett.65.2298>.

[8] D. Braithwaite, M. Vališka, G. Knebel, G. Lapertot, J. P. Brison, A. Pourret, M. E. Zhitomirsky, J. Flouquet, F. Honda, and D. Aoki, Communications Physics **2**, 147 (2019), URL <https://www.nature.com/articles/s42005-019-0248-z>.

[9] D. Aoki, F. Honda, G. Knebel, D. Braithwaite, A. Nakamura, D. Li, Y. Homma, Y. Shimizu, Y. J. Sato, J.-P. Brison, et al., J. Phys. Soc. Jpn. **89**, 053705 (2020), URL <https://journals.jps.jp/doi/10.7566/JPSJ.89.053705>.

[10] K. Kinjo, H. Fujibayashi, S. Kitagawa, K. Ishida, Y. Tokunaga, H. Sakai, S. Kambe, A. Nakamura, Y. Shimizu, Y. Homma, et al., arXiv: 2206.02444, URL <https://arxiv.org/abs/2206.02444>.

[11] H. Sakai, Y. Tokiwa, P. Opletal, M. Kimata, S. Awaji, T. Sasaki, D. Aoki, S. Kambe, Y. Tokunaga, and Y. Haga, arXiv: 2210.05909, URL <https://arxiv.org/abs/2210.05909>.

[12] A. W. W. Ludwig and I. Affleck, Phys. Rev. Lett. **67**, 3160 (1991), URL <https://link.aps.org/doi/10.1103/PhysRevLett.67.3160>.

[13] M. Kibune, S. Kitagawa, K. Kinjo, S. Ogata, M. Manago, T. Taniguchi, K. Ishida, M. Brando, E. Hassinger, H. Rosner, et al., Phys. Rev. Lett. **128**, 057002 (2022), URL <https://link.aps.org/doi/10.1103/PhysRevLett.128.057002>.

[14] J. F. Landaeta, P. Khanenko, D. C. Cavanagh, C. Geibel, S. Khim, S. Mishra, I. Sheikin, P. M. R. Brydon, D. F. Agterberg, M. Brando, et al., Phys. Rev. X **12**, 031001 (2022), URL <https://journals.aps.org/prx/abstract/10.1103/PhysRevX.12.031001>.

[15] D. C. Cavanagh, T. Shishidou, M. Weinert, P. M. R. Brydon, and D. F. Agterberg, Phys. Rev. B **105**, L020505 (2022), URL <https://journals.aps.org/prb/abstract/10.1103/PhysRevB.105.L020505>.

[16] T. Yoshida, M. Sigrist, and Y. Yanase, Phys. Rev. B **86**, 134514 (2012), URL <https://journals.aps.org/prb/abstract/10.1103/PhysRevB.86.134514>.

[17] M. Sigrist, D. F. Agterberg, M. H. Fischer, J. Goryo, F. Loder, S.-H. Rhim, D. Maruyama, Y. Yanase, T. Yoshida, and S. J. Youn, J. Phys. Soc. Jpn. **83**, 061014 (2014), URL <https://journals.jps.jp/doi/full/10.7566/JPSJ.83.061014>.

[18] D. Möckli, Y. Yanase, and M. Sigrist, Phys. Rev. B **97**, 144508 (2018), URL <https://link.aps.org/doi/10.1103/PhysRevB.97.144508>.

[19] E. G. Schertenleib, M. H. Fischer, and M. Sigrist, Phys. Rev. Research **3**, 023179 (2021), URL <https://journals.aps.org/prresearch/abstract/10.1103/PhysRevResearch.3.023179>.

[20] A. Skurativska, M. Sigrist, and M. H. Fischer, Phys. Rev. Res. **3**, 033133 (2021), URL <https://journals.aps.org/prresearch/abstract/10.1103/PhysRevResearch.3.033133>.

[21] K. Nogaki, A. Daido, J. Ishizuka, and Y. Yanase, Phys. Rev. Res. **3**, L032071 (2021), URL <https://journals.aps.org/prresearch/abstract/10.1103/PhysRevResearch.3.L032071>.

[22] K. Nogaki and Y. Yanase, Phys. Rev. B **106**, L100504 (2022).

[23] S. Mishra, Y. Liu, E. D. Bauer, F. Ronning, and S. M. Thomas, Phys. Rev. B **106**, L140502 (2022), URL <https://journals.aps.org/prb/abstract/10.1103/PhysRevB.106.L140502>.

[24] K. Machida, Phys. Rev. B **106**, 184509 (2022), URL <https://journals.aps.org/prb/abstract/10.1103/PhysRevB.106.184509>.

[25] O. P. Squire, S. A. Hodgson, J. Chen, V. Fedoseev, C. K. de Podesta, T. I. Weinberger, P. L. Alireza, and F. M. Grosche, arXiv: 2211.00975, URL <https://arxiv.org/abs/2211.00975>.

[26] S. Onishi, U. Stockert, S. Khim, J. Banda, M. Brando, and E. Hassinger, Frontiers in Electronic Materials **2** (2022), ISSN 2673-9895, URL <https://www.frontiersin.org/articles/10.3389/femat.2022.880579/full>.

[27] M. D. Bachmann, G. M. Ferguson, F. Theuss, T. Meng, C. Putzke, T. Helm, K. R. Shirer, Y.-S. Li, K. A. Modic, M. Nicklas, et al., Science **366**, 221 (2019), ISSN 0036-8075, URL <https://www.science.org/doi/10.1126/science.aa06640>.

[28] S. K. Yip, T. Li, and P. Kumar, Phys. Rev. B **43**, 2742 (1991), URL <https://link.aps.org/doi/10.1103/PhysRevB.43.2742>.

[29] Y. Imry, Journal of Physics C: Solid State Physics **8**, 567 (1975), URL <https://dx.doi.org/10.1088/0022-3719/8/5/005>.

[30] R. M. Fernandes and J. Schmalian, Phys. Rev. B **82**, 014521 (2010), URL <https://link.aps.org/doi/10.1103/PhysRevB.82.014521>.

[31] F. Pobell, *Matter and Methods at Low Temperatures* (Springer-Verlag, 2007).

- [32] A. Steppke, M. Brando, N. Oeschler, C. Krellner, C. Geibel, and F. Steglich, *Phys. Status Solidi (b)* **247**, 737 (2010), URL <https://onlinelibrary.wiley.com/doi/abs/10.1002/pssb.200983062>.
- [33] T. Hagino, Y. Seki, S. Takayanagi, N. Wada, and S. Nagata, *Phys. Rev. B* **49**, 6822 (1994), URL <https://link.aps.org/doi/10.1103/PhysRevB.49.6822>.
- [34] T. Grüner, D. Jang, Z. Huesges, R. Cardoso-Gil, G. H. Fecher, M. M. Koza, O. Stockert, A. Mackenzie, M. Brando, and C. Geibel, *Nat. Phys.* **13**, 967 (2017), URL <https://doi.org/10.1038/nphys4191>.